

A first-order phase transition at the random close packing of hard spheres

Yuliang Jin and Hernán A. Makse

*Levich Institute and Physics Department,
City College of New York, New York, NY 10031, US*

Abstract

Randomly packing spheres of equal size into a container consistently results in a static configuration with a density of $\sim 64\%$. The ubiquity of random close packing (RCP) rather than the optimal crystalline array at 74% begs the question of the physical law behind this empirically deduced state. Indeed, there is no signature of any macroscopic quantity with a discontinuity associated with the observed packing limit. Here we show that RCP can be interpreted as a manifestation of a thermodynamic singularity, which defines it as the “freezing point” in a first-order phase transition between ordered and disordered packing phases. Despite the athermal nature of granular matter, we show the thermodynamic character of the transition in that it is accompanied by sharp discontinuities in volume and entropy. This occurs at a critical compactivity, which is the intensive variable that plays the role of temperature in granular matter. Our results predict the experimental conditions necessary for the formation of a jammed crystal by calculating an analogue of the “entropy of fusion”. This approach is useful since it maps out-of-equilibrium problems in complex systems onto simpler established frameworks in statistical mechanics.

Since the time of Kepler it is thought that the most efficient packing of monodisperse spherical grains is the face centered cubic (FCC) arrangement with a density of 74 % [1]. Thus, we might expect that spherical particles will tend to optimize the space they occupy by crystallizing up to this limiting density. Instead, granular systems of spheres arrest in a random close packing (RCP), which is not optimal but occupies $\sim 64\%$ of space [2]. Previous studies have derived geometric statistical models to map the microscopic origin of the much debated 64% density of RCP [2–9]. However, the physical laws that govern its creation and render it the most favorable state for randomly packed particles remains one of the most salient questions in understanding all of jammed matter [3–5, 8]. For instance, while it is known that systems in equilibrium follow energy minimization and entropy maximization to reach a steady state, the mechanism by which RCP is achieved is much sought after.

Here we propose a thermodynamic view of the sphere packing problem where the experimentally observed RCP can be viewed as a manifestation of a singularity in a first-order phase transition. Despite the inherent out-of-equilibrium nature of granular matter, the formation of a jammed crystal can be mapped to a thermodynamic process that occurs at a precise compactivity where the volume and entropy are discontinuous.

We investigate mechanically stable packings ranging from the lowest possible volume fraction of random loose packing (RLP) [10] to FCC. We numerically generate packings of $N = 10,000$ spherical particles of radius $R = 100\mu\text{m}$ in a periodically repeated cube. Initially, we use the Lubachevsky-Stillinger (LS) [11, 12] and force-biased (FBA) [13] algorithms to generate amorphous configurations of unjammed hard-spheres fluids at infinite kinetic pressure and volume fraction ϕ_i [6, 12] (see Appendix-Section I). While these configurations are geometrically jammed, they are not jammed in a mechanical sense since the particles do not carry any forces: the confining stress σ (not kinetic) is zero. In fact a key difference between granular materials jammed under external stress or gravity and hard-sphere fluids is that, in the former, each particle satisfies force and torque balance. In order to study mechanically stable packings characterized by a jamming transition we introduce interparticle forces via the Hertz-Mindlin model of normal and tangential forces allowing the particles to be soft but with a large Young modulus, Y . We then simulate the process of jamming by Molecular Dynamics (MD) simulations using previously developed methods [14] to compress the LS and FBA packings from ϕ_i to a final jamming density, ϕ_j . Ultimately, we obtain mechanically stable packings just above the jamming transition (in the limit of vanishingly small

confining stress, or equivalently in the hard-sphere limit, $\sigma/Y \rightarrow 0^+$) covering a range of ϕ_j from $\phi_{\text{rlp}} = 0.55$ to crystallization at $\phi_{\text{fcc}} = 0.74$.

The mechanical coordination number averaged over all the particles in a packing, Z_j , characterizes different states of granular matter [2, 7, 15]. Therefore, our study begins by plotting Z_j versus ϕ_j for all generated packings. Figure 1 suggests the existence of a transition occurring at RCP evidenced by the abrupt plateau in Z_j . This transition could be thought of as an analogue to the classical hard sphere liquid-solid phase transition in thermal equilibrium [16, 17]. Such an analogy becomes apparent if one identifies Z_j of the jammed packing with the kinematic pressure of the equilibrium hard sphere system [6] and it is in agreement with a recent conjecture regarding the definition of RCP [8].

Figure 1 identifies two branches and a coexistence region: (i) An ordered branch of crystallized states with ϕ_j ranging from 0.68 to a FCC lattice at 0.74. (ii) A disordered branch within $0.55 \sim 0.64$ which can be fitted with the statistical theory of [7]: $\phi_j = Z_j/(Z_j + 2\sqrt{3})$ as shown in the figure. (iii) A coexistence region between 0.64 to 0.68 displaying a plateau at the isostatic coordination number, $Z_{\text{iso}} = 6$ [4, 14, 18]. The intersection between the disordered branch and the coexistence line identifies the “freezing point” of the transition providing a definition of RCP. Using the theoretical results of [7], freezing occurs at $Z_{\text{iso}} = 6$ and $\phi_{\text{rcp}} = 6/(6 + 2\sqrt{3}) \approx 0.634$. The corresponding “melting point” appears at the other end of the coexistence at $\phi_{\text{melt}} = 0.68$, signaling the beginning of the ordered branch. Finite size analysis is shown in the Appendix-Fig. 5A: the results for 500 and 10,000 spheres are consistent with each other. Other geometric aspects of the transition are discussed in Appendix-Section II.

To reveal the nature of the newly found phases we start with a descriptive viewpoint and then turn to a thermodynamic analysis to model the transition. In order to investigate if the concept of phase transition applies to the trend observed in Z_j , one commonly looks at the global (Q_l, W_l) , and local (q_6) orientational order parameters for a signature of varying amounts of crystallization present in the packings as defined elsewhere [19] (see Appendix-Section III A and Fig. 2 for definitions). The salient feature of Q_l is that its zero value means disorder and non-zero value means crystallization. Therefore, the presence in Fig. 2A of an increase in Q_l from zero at ϕ_{rcp} defines the beginning of the coexistence region. Typically, a first-order transition is marked by a nonzero third-order invariant W_l [19, 20] which we find appears at the melting point ϕ_{melt} signaling the onset of the ordered branch

(Fig. 2B).

Interestingly, the ordered phase has two significant peaks in the probability distribution $P(q_6)$ of the local order parameter of each particle, q_6 (Fig. 2C). The peaks correspond to FCC and HCP [19] signaling that both crystalline configurations are present in the ordered structure. From the available data we cannot rule out the possibility of another transition from HCP to FCC before $\phi_j \sim 0.74$. The Gaussian distributions $P(q_6)$ obtained for ϕ_j within $0.55 \sim 0.64$ show no preferred lattice structure in the random branch. While the relative peak positions in $P(q_6)$ do not change, the percentage of crystal and random phase found in the packing progresses from one to the other in the coexistence region. Microscopically, the existence of the two pure phases is starkly represented by the two separated distributions of local Voronoi volume fractions $P(\phi_{\text{vor}})$ for which the same phenomenology of $P(q_6)$ applies (Fig. 2D, $\phi_{\text{vor}} = V_g/V_{\text{vor}}$, where V_{vor} is the Voronoi volume [7, 15] of each particle of volume V_g). This descriptive analysis is further supported in Appendix-Section III.

Having identified the structure of the phases we now develop a thermodynamic viewpoint of the RCP transition to rationalize the obtained results. Transitions in equilibrium physical systems are driven by a competition of energy and entropy. Instead, a transition in athermal jammed matter is driven by the minimization of the system's volume W by compactification and entropy maximization of jammed configurations [21, 22]. In accordance with the second law of thermodynamics, the granular system tends to minimize its Gibbs-Helmholtz “free energy” $F = W - XS$ rather than W alone. The compactivity of the system $X = dW/dS$ is a measure of how much further compaction a packing can undergo; the lower the volume the lower the compactivity [21]. Thus, we map the packing problem to a thermodynamic problem where the volume W replaces the energy and X takes the role of temperature. The principle of free energy minimization can thus be applied.

The equations of state, $\phi_j(X)$ and $S(\phi_j)$, can be calculated from the fluctuations of the Voronoi volumes in the disordered and ordered phases [23], $\sigma_1(\phi_j)$ and $\sigma_2(\phi_j)$ respectively, in analogy to the standard Boltzmann statistical mechanics ($\sigma^2 \equiv \langle w_{\text{vor}}^2 \rangle - \langle w_{\text{vor}} \rangle^2$ and $\omega_{\text{vor}} = 1/\phi_{\text{vor}} = V_{\text{vor}}/V_g$ is the reduced Voronoi volume). Figure 3A shows clearly the existence of the two pure phases and a discontinuity between both branches. We obtain the compactivity by integration of σ_1 and σ_2 using Einstein fluctuation theory [23–25] (see Appendix-Section IV A for more details, we set $k_B = 1$ for simplicity, X is given in units of

V_g and entropy is dimensionless):

$$\frac{1}{X(\phi_j)} = \frac{1}{V_g} \int_{\phi_{\text{rlp}}}^{\phi_j} \frac{d\phi}{\phi^2 \sigma_1^2(\phi)} + \frac{1}{X_{\text{rlp}}}, \quad \phi_{\text{rlp}} \leq \phi_j \leq \phi_{\text{rcp}}, \quad (1a)$$

$$\frac{1}{X(\phi_j)} = \frac{1}{V_g} \int_{\phi_{\text{melt}}}^{\phi_j} \frac{d\phi}{\phi^2 \sigma_2^2(\phi)} + \frac{1}{X_{\text{melt}}}, \quad \phi_{\text{melt}} \leq \phi_j \leq \phi_{\text{fcc}}, \quad (1b)$$

where $X_{\text{melt}} = X(\phi_{\text{melt}})$ and $X_{\text{rlp}} = X(\phi_{\text{rlp}})$ are the compactivities at the melting point and at RLP, respectively. Once $X(\phi_j)$ is obtained from Eq. (1), the entropy density, $s = S/N$, is calculated by integration [23] (see Appendix-Section IV A):

$$s(\phi_j) = s_{\text{rcp}} + V_g \int_{\phi_j}^{\phi_{\text{rcp}}} \frac{d\phi}{X(\phi)\phi^2}, \quad \phi_{\text{rlp}} \leq \phi_j \leq \phi_{\text{rcp}}, \quad (2a)$$

$$s(\phi_j) = V_g \int_{\phi_j}^{\phi_{\text{fcc}}} \frac{d\phi}{X(\phi)\phi^2}, \quad \phi_{\text{melt}} \leq \phi_j \leq \phi_{\text{fcc}}, \quad (2b)$$

where we have used that the entropy of FCC is zero in the thermodynamic limit. There are three unknown integration constants in Eqs. (1) and (2): X_{rlp} , X_{melt} and the entropy of RCP, s_{rcp} . To close the system, we consider the conditions for equilibrium between the phases [21]: (a) ‘‘thermal’’ equilibrium $X_{\text{melt}} = X_{\text{rcp}} \equiv X_c$, where X_c is the critical compactivity at the transition, and (b) the equality of the free energy density (or chemical potential), $f = F/N$, at the melting and the freezing RCP point: $f_{\text{melt}} = f_{\text{rcp}}$. This implies, $\omega_{\text{rcp}} - (X_c/V_g)s_{\text{rcp}} = \omega_{\text{melt}} - (X_c/V_g)s_{\text{melt}}$, where $w = 1/\phi_j = W/(NV_g)$ is the reduced volume of the system. The third integration constant X_{rlp} can be considered infinite [7, 23, 25] since RLP is the highest volume of the system. While the precise value of X_{rlp} does not affect our conclusions, a more accurate finite value can be obtained by fitting the entropy Eq. (2) with an independent measure obtained by cluster analysis from information theory (Shannon entropy, s_{shan}) as developed in [23] (Appendix-Section IV B). Figure 3B shows that the entropy from the thermodynamic integration Eq. (2) and s_{shan} agree well (up to a multiplicative constant) supporting the framework of Eqs. (1)-(2). The entropy is composed of two branches plus the coexistence region (green line in Fig. 3B).

Figure 4A displays a discontinuity in $s(X)$ at $X_c = 0.031V_g$ revealing the first-order nature of the transition which is accompanied by an ‘‘entropy of fusion’’ $\Delta s_{\text{fus}} \equiv s_{\text{rcp}} - s_{\text{melt}} = 3.0$. The volume fraction is discontinuous at X_c (Fig. 4B) where the system jumps from RCP to the melting point releasing an amount of volume given by the ‘‘enthalpy of fusion’’ $\Delta h_{\text{fus}} =$

$X_c \Delta s_{\text{fus}} = 0.09V_g$ while the compactivity stays constant. This process corresponds to the typical latent heat in exothermic first-order transitions.

Systems jammed at RCP need to overcome a volume barrier Δh_{fus} for crystal formation or, equivalently, particle displacements $\Delta r_{\text{fus}} \approx 0.45R$. From a thermodynamic perspective, the requirement is equivalent to bringing a random packing in contact with a compactivity bath at $X < X_c = 0.031V_g$. The fundamental idea is to surround a random packing above X_c with a crystal lattice below X_c and perturb the system to equilibrate. A shear cycling experiment—which conserves the shape of the box containing the particles—suffices to explore the crystal branch [26, 27]. Shear-induced crystallization has been observed [26, 27] when the maximum angle of horizontal shear is above $\theta \approx 10^\circ$. This value is of the same order as our estimate of the shear amplitude to crystallize at $\phi_j = 68\%$ based on the entropy of fusion, which gives $\theta \equiv \tan^{-1}(\Delta r_{\text{fus}}/2R) \approx 13^\circ$. Furthermore, recent shear cycling experiments [8, 28] appear to be in reasonable agreement with the present results. We also expect that 2d equal-sized disks may have a near zero entropy of fusion owing to their tendency to easily crystallize while Δs_{fus} may sharply increase in 4d and above [6].

The behavior of the free energy density shown in Figs. 4C and 4D summarizes the mechanism to achieve RCP. The free energy in Fig. 4C increases as X decreases from RLP to freezing at RCP. At X_c , the system transitions to the phase with the lower free energy through an entropy discontinuity given by $s = -\partial f/\partial X$. The system may also enter the metastable branch as indicated in Fig. 4C and in Figs. 1 and 3B from $a \rightarrow b$. In the spirit of Landau mean field theory of phase transitions, we relate the distribution of the local order parameter to the free energy functional, \mathcal{F} , and X as $P(q_6) \approx \exp[-\mathcal{F}(q_6)/X]$ [20]. Figure 4D shows $\mathcal{F}(q_6)$ displaying the minima of $\mathcal{F}(q_6)$ defining the order and disorder phases at different ϕ_j . We find that the location of the minimum at $q_6^{\text{min}} \approx 0.425$ remains constant from RLP up to the freezing point as expected in the disordered phase. The value of $\mathcal{F}(q_6^{\text{min}})$ is very deep for $\phi_j = 0.55$ and becomes less deep as the freezing point is approached. The value of $\mathcal{F}(q_6^{\text{min}})$ at the freezing and melting points become approximately equally deep indicating the phase coexistence at X_c . Within a statistical mechanics framework, these results are a natural consequence and give support to such an underlying statistical picture.

In conclusion, treating granular packings from the perspective of theoretical physics developed by Boltzmann and Gibbs has the potential to answer basic questions in the field of disordered media. State variables like the compactivity can be introduced with the potential

of identifying transition points between different phases, a fact that can unequivocally define RCP as the freezing point in a discontinuous transition. This formalism may be useful in analyzing other related transitions in complex systems ranging from optimization problems in computer science [29] to the physics of glasses [6]. Other unsolved packing problems including finding the densest arrangement of rods, ellipsoids, spherocylinders, binary mixtures, Platonic and Archimedean solids—which are known to pack better than spheres [9, 30]—can now be analyzed from the proposed thermodynamic view of phase transitions.

-
- [1] T. Aste, D. Weaire, *The pursuit of perfect packing* (Taylor & Francis, 2008).
- [2] J. D. Bernal, J. Mason, *Nature* **188**, 910 (1960).
- [3] S. Torquato, T. M. Truskett, P. G. Debenedetti, *Phys. Rev. Lett.* **84**, 2064 (2000).
- [4] C. S. O'Hern, L. E. Silbert, A. J. Liu, S. R. Nagel, *Phys. Rev. E* **68**, 011306 (2003).
- [5] R. D. Kamien, A. J. Liu, *Phys. Rev. Lett.* **99**, 155501 (2007).
- [6] G. Parisi, F. Zamponi, to be published in *Rev. Mod. Phys.* Arxiv preprint at www.arxiv.org/abs/0802.2180 (2009).
- [7] C. Song, P. Wang, H. A. Makse, *Nature* **453**, 629 (2008).
- [8] C. Radin, *J. Stat. Phys.* **131**, 567 (2008).
- [9] M. Clusel, E. I. Corwin, A. O. N. Siemens, J. Brujić, *Nature* **460**, 611 (2009).
- [10] G. Y. Onoda, E. G. Liniger, *Phys. Rev. Lett.* **64**, 2727 (1990).
- [11] B. D. Lubachevsky and F. H. Stillinger, *J. Stat. Phys.* **60**, 561 (1990).
- [12] M. Skoge, A. Donev, F. H. Stillinger, S. Torquato, *Phys. Rev. E* **74**, 041127 (2006).
- [13] J. Moscinski, M. Bargiel, Z. A. Rycerz, P. W. M. Jacobs, *Mol. Sim.* **3**, 201 (1989).
- [14] H. A. Makse, D. L. Johnson, L. M. Schwartz, *Phys. Rev. Lett.* **84**, 4160 (2000).
- [15] T. Aste, M. Saadatfar, T. J. Senden, *J. Stat. Mech.*, P07010 (2006).
- [16] B. Alder, T. Wainwright, *J. Chem. Phys.* **27**, 1208 (1957).
- [17] P. G. Debenedetti, *Metastable liquids: Concepts and Principles* (Princeton University Press, Princeton, 1996).
- [18] C. F. Moukarzel, *Phys. Rev. Lett.* **81**, 1634 (1998).
- [19] P. J. Steinhardt, D. R. Nelson, M. Ronchetti, *Phys. Rev. B* **28**, 784 (1983).
- [20] K. Binder, *Rep. Prog. Phys.* **50**, 783 (1987).
- [21] S. F. Edwards, The role of entropy in the specification of a powder, in *Granular matter: an interdisciplinary approach* (ed. A. Mehta) 121-140 (Springer-Verlag, New York, 1994).
- [22] M. P. Ciamarra, A. Coniglio, M. Nicodemi, *Phys. Rev. Lett.* **97**, 158001 (2006).
- [23] C. Briscoe, C. Song, P. Wang, H. A. Makse, *Phys. Rev. Lett.* **101**, 188001 (2008).
- [24] E. R. Nowak, J. B. Knight, E. Ben-Naim, H. M. Jaeger, S. R. Nagel, *Phys. Rev. E* **57**, 1971 (1998).
- [25] M. Schröter, D. I. Goldman, H. L. Swinney, *Phys. Rev. E* **71**, 030301(R) (2005).

- [26] G. D. Scott, A. M. Charlesworth, M. K. Mak. *J. Chem. Phys.* **40**, 611 (1964).
- [27] M. Nicolas, P. Duru, O. Poulliquen, *Eur. Phys. J. E* **3**, 309 (2000).
- [28] F. Rietz, private communication. Bulletin of the American Physical Society, **54**, Number 19, AU.00006 (2009).
- [29] F. Krzakala, J. Kurchan, *Phys. Rev. E* **76**, 021122 (2007).
- [30] A. Haji-Akbari, *et al.*, *Nature* **462**, 773 (2009).

Acknowledgements. This work is supported by the National Science Foundation. We are grateful to B. Brujić, M. Shattuck, F. Zamponi, C. Song and P. Wang for discussions.

FIG. 1. The RCP transition. We plot the mechanical coordination number Z_j versus the volume fraction ϕ_j for each packing. We identify: (i) a disordered branch which can be fitted with the statistical model of [7] as shown, (ii) a coexistence region, and (iii) an ordered branch. Error bars are calculated over 523 packings obtained from initial LS configurations. The 3d plots visualize how the transition occurs in terms of arrangements of contacting particles. White particles are random clusters, light blue are HCP and green are FCC clusters. Further microscopic information regarding the transition is provided in Appendix-Section II B.

FIG. 2. Descriptive viewpoint of the RCP transition. **(A)** Global orientational order parameters Q_l versus ϕ_j for different packings signaling the freezing point at ϕ_{rcp} . A linear fit is possible in the coexistence region. **(B)** Global third-order invariants W_l versus ϕ_j signaling the melting point at ϕ_{melt} . **(C)** Probability distribution of local orientational order parameter $P(q_6)$ versus q_6 (vertical axis) for packings with ϕ_j (horizontal axis). For packings with ϕ_j within $0.68 \sim 0.72$, the distributions have two significant peaks centered at $q_6^{\text{fcc}} = 0.57$ and $q_6^{\text{hcp}} = 0.48$, which correspond to FCC and HCP arrangements, respectively [19]. Color bar indicates the values of $P(q_6)$. Since the peaks are very pronounced, we plot $P(q_6)$ up to the indicated value. **(D)** Probability distribution of local volume fractions of the Voronoi volumes of each particle, $P(\phi_{\text{vor}})$ versus ϕ_{vor} (vertical axis) for different ϕ_j (horizontal axis). The plot indicates a clear discontinuity between both branches. Color bar indicates the values of $P(\phi_{\text{vor}})$ which are plotted up to the indicated value.

FIG. 3. Equations of state of the RCP transition. **(A)** Volume fluctuations of the Voronoi cell of a particle as a function of ϕ_j . The data indicates a discontinuity between the ordered and disordered branches which are fitted by functions as indicated. These fittings are used in the integrations of Eq. (1). The larger fluctuations in volume observed in the order state compared to the disorder state at similar ϕ_j are due to the fact that the system packs better in the former and thus displays larger fluctuations when the system volume is the same. **(B)** Entropy obtained from fluctuation theory in Eq. (2), s , and Shannon entropy from information theory, s_{shan} , versus volume fraction ϕ_j . Both entropies agree (up to a multiplicative constant, $k = 0.1$, as indicated) confirming our calculations. The extended branch denotes a metastable state ending at point b at an hypothetical Kauzmann density, ϕ_K , in analogy with the physics of glasses [6] (see Appendix-Section II C).

FIG. 4. Thermodynamic viewpoint of the RCP transition. All the observables are con-

sistent with a transition at $X_c = 0.031V_g$. **(A)** Entropy s versus X . **(B)** Volume fraction ϕ_j versus X . **(C)** Free energy density f versus X . We extend f for both branches to indicate the possible metastable states. At X_c the system follows the minimization of the free energy signaling the transition from RCP to order. **(D)** Free energy functional $\mathcal{F}(q_6)$ versus q_6 (vertical axis) ϕ_j (horizontal axis). Color bar indicates the values of $\mathcal{F}(q_6)$, which are plotted in the range indicated to focus on the region of coexistence. The minima correspond to the disordered phase and the FCC and HCP phases in the ordered branch.

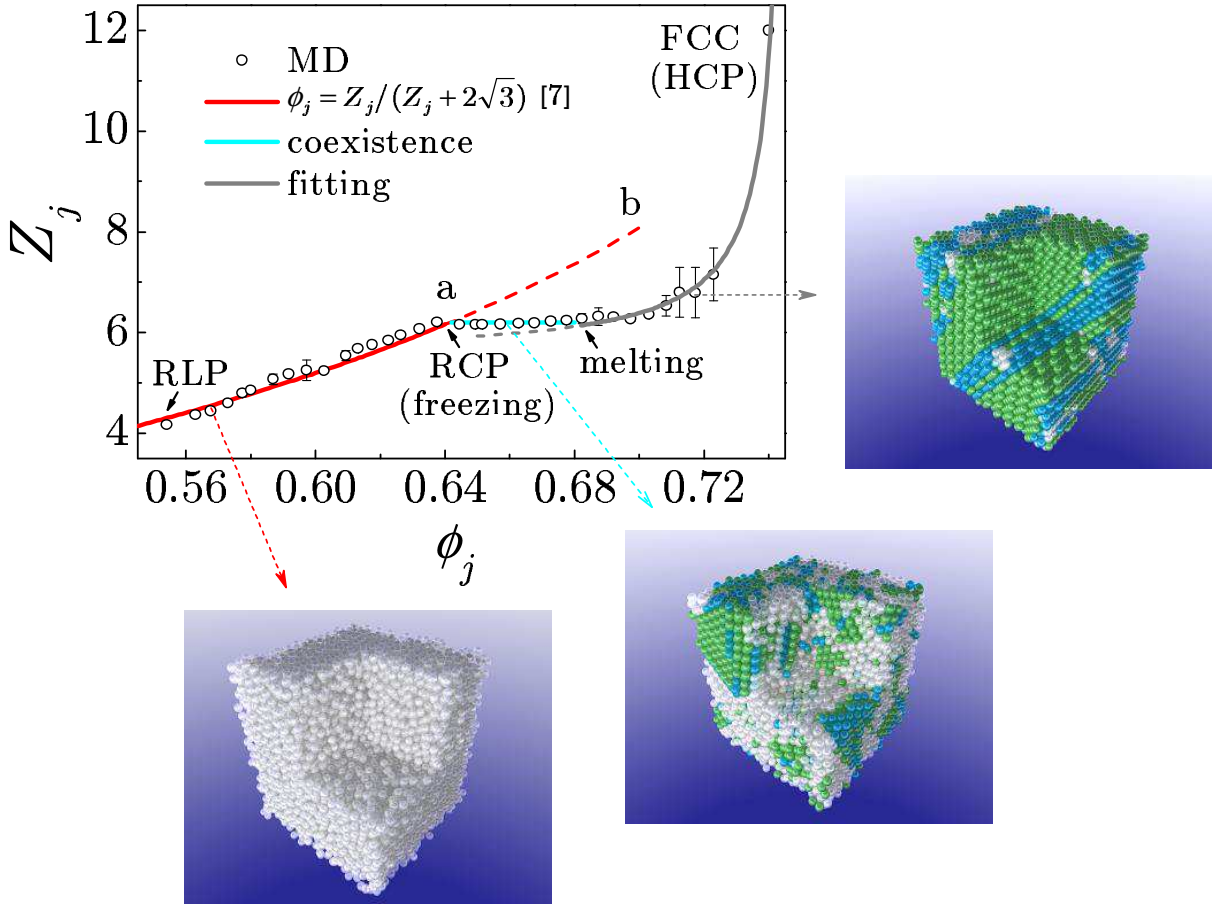


FIG. 1:

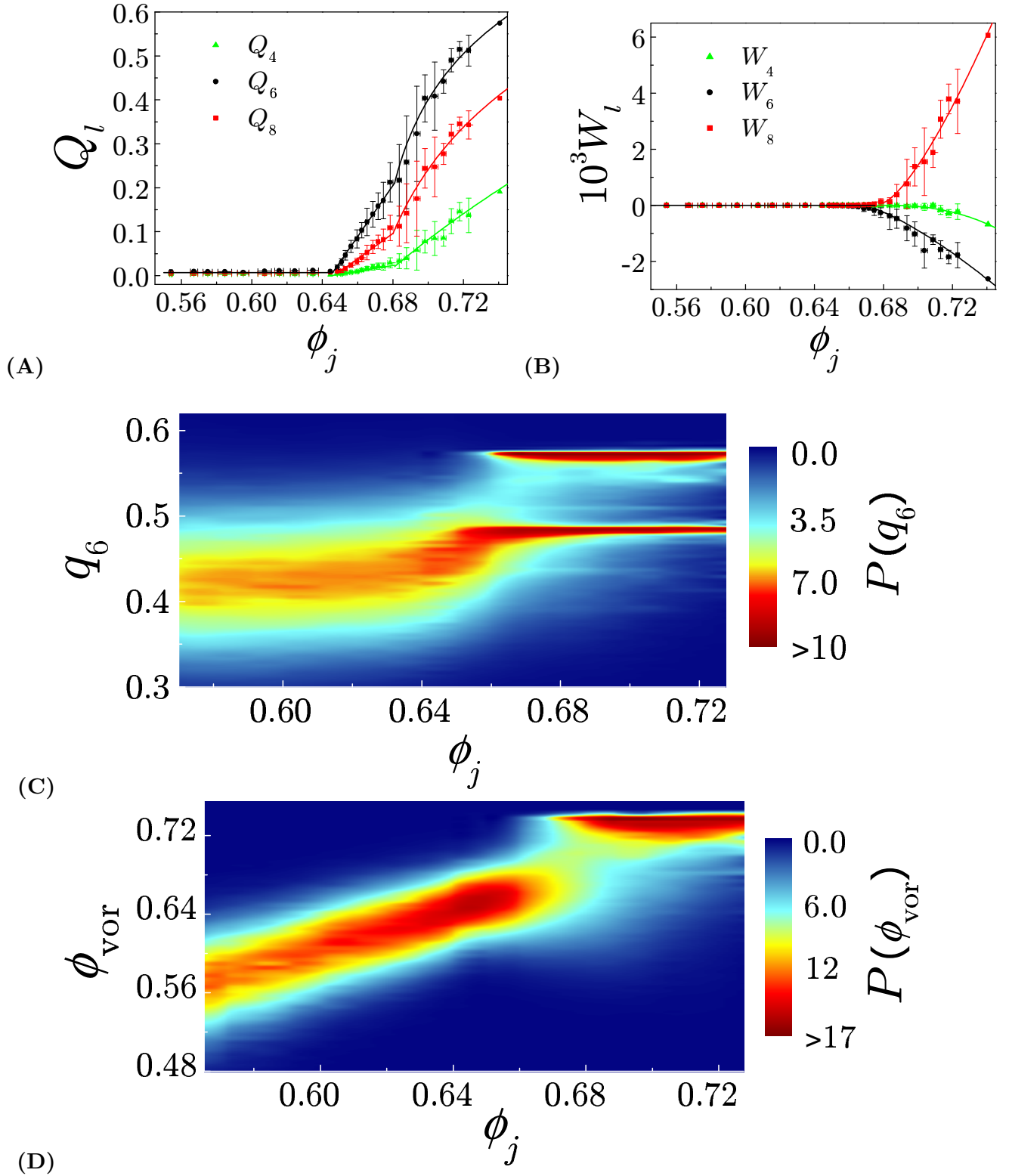
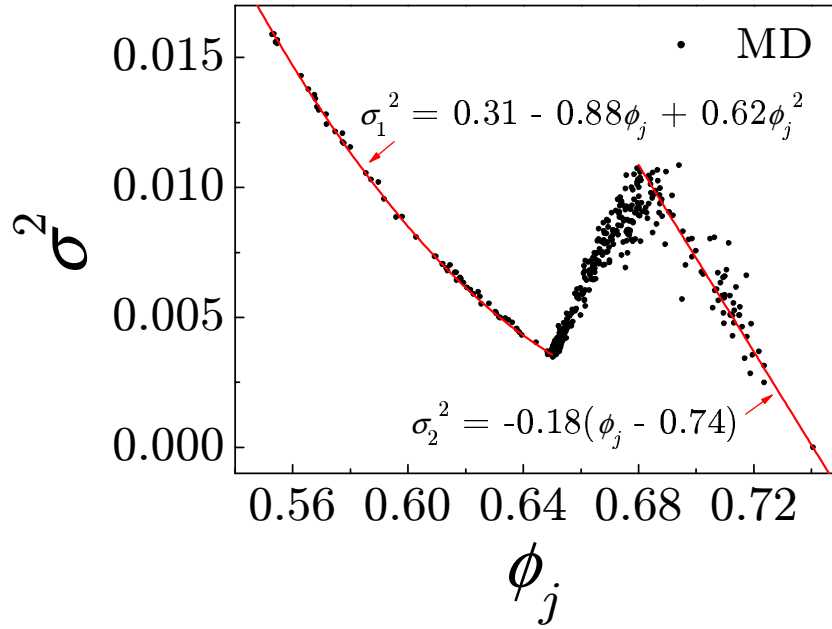
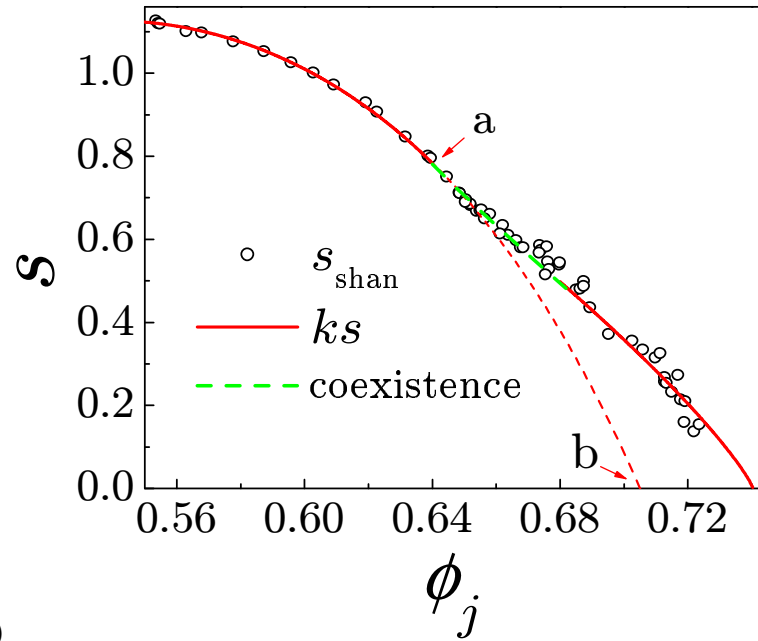


FIG. 2:



(A)



(B)

FIG. 3:

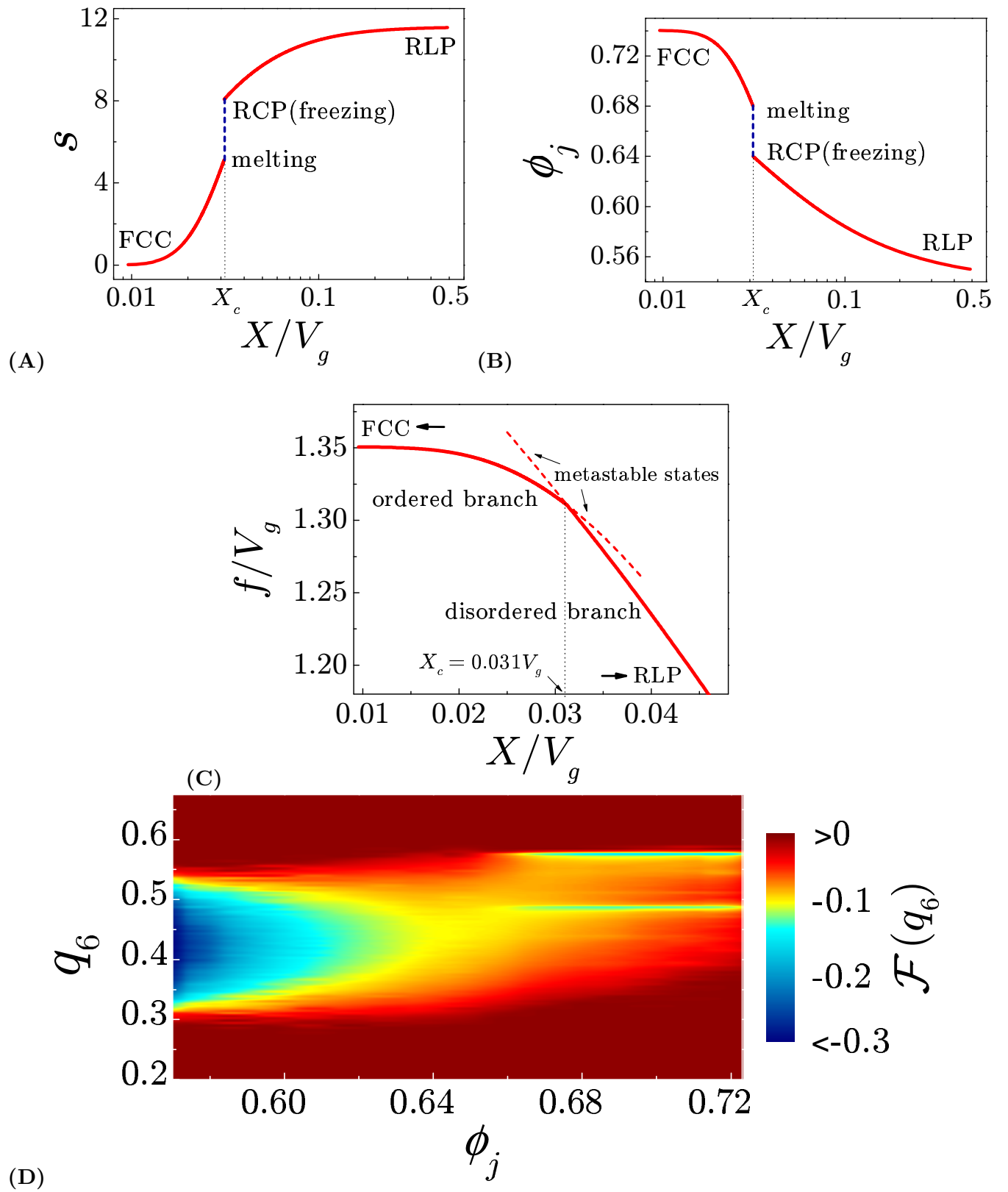


FIG. 4:

Appendix

A first order phase transition at the random close packing of hard spheres

Yuliang Jin and Hernán A. Makse

Here, we describe the details of the MD simulations (Section I), geometrical interpretations of the transition (Section II), and the calculations leading to the descriptive (Section III) and the thermodynamic (Section IV) view of the RCP transition.

I. ALGORITHM

We use computer simulations to obtain jammed packings containing $N = 10,000$ monodisperse spheres of radius $R = 100\mu\text{m}$ with periodic boundary conditions. We first apply a modified Lubachevsky-Stillinger (LS) algorithm [11, 12] to generate packings of densities up to ~ 0.72 . In the algorithm, a set of random distributed points grow into nonoverlapping spheres at a fixed expansion rate γ . The spheres are considered perfectly elastic and evolve in time according to Newtonian dynamics. The configurations eventually arrive at out-of-equilibrium states with a diverging collision rate and a density ϕ_i . Practically, we set the reduced kinetic pressure of the fluid defined as $p = PV/Nk_B T$ to be 10^{12} [12] as a criteria of the diverging collision rate. The final packing configurations depend on the expansion rate γ : large values of expansion rate result in random packings with very low packing densities, while small values of expansion rate result in packings with higher densities.

Although the packings obtained from the modified LS algorithm are considered as “geometrically jammed”, they are not jammed in the mechanical sense since the particles do not carry on any forces. In order to study mechanical stable packings characterized by a jamming transition, we model the microscopic interaction between deformable grains by the nonlinear Hertz-Mindlin normal and tangential forces [7, 14]. We use configurations from the modified LS as the starting point, ϕ_i , and apply molecular dynamics to simulate Newton equations for the evolution of the particles following algorithms in [7, 14].

The aim of this part of the protocol is to generate mechanically stable jammed packings at the jamming transition ϕ_j . For the packings obtained by the LS algorithm, we first reset the velocities of the particles to zero. At this point the system stress σ and mechanical coordination number Z_j are zero since there is no deformation or overlapping between the

particles. We notice that the stress σ is not the kinetic pressure, p , measured in the LS packings which diverges at the end of the LS protocol. Here σ refers to the mechanical pressure related to the trace of the stress tensor σ_{ij} via $\sigma = \sigma_{ii}/3$, where

$$\sigma_{ij} = \frac{R}{2V} \sum_{\text{contacts}} f_i^c n_j^c + f_j^c n_i^c, \quad (3)$$

where the sum is over all the contact forces, f_i^c denotes the i -th component of the contact force, $\hat{\mathbf{n}}^c$ is the unit vector joining the center of two spheres of radius R in contact and V is the system volume.

The system is then compressed isotropically by a constant compression rate until a given nonzero stress σ is reached. Next, we turn off the compression and allow the system to relax with constant volume. If the system eventually reaches a jammed state with a fixed nonzero σ and coordination number, the system pressure will remain unchanged over a large period of time (usually $\sim 10^7$ MD steps); otherwise, if the system is not stable, the pressure will relax to zero very fast [7].

Previous studies show that there exists a jamming transition for granular matter as

$$\sigma(\phi) - \sigma_j \sim (\phi - \phi_j)^\alpha, \quad (4)$$

and

$$Z(\phi) - Z_j \sim (\phi - \phi_j)^\beta. \quad (5)$$

Here, σ_j is zero for frictionless packings. However, it could have nonzero value for frictional packings, in general. The exponent $\alpha = 3/2$ is trivially related to the Hertz-law of interparticle contact force and $\beta = 1/2$ seems to be universal over different force laws [4].

In practice, it is difficult to reach a jammed packing exactly at the transition point ϕ_j while it is much easier to get a stable packing with slightly higher pressure. In order to approach the transition point, a jammed packing at higher pressure than σ_j in Eq. (4) obtained using the above protocol is decompressed with a negative compression rate until certain lower pressure is reached. Then the system is allowed to relax again to check for mechanical stability. If it is stable, then the system is decompressed further to an even lower pressure, and we check its stability again. By this process (called the split algorithm in [7]) we are able to approach the density ϕ_j at the jamming transition point as close as possible

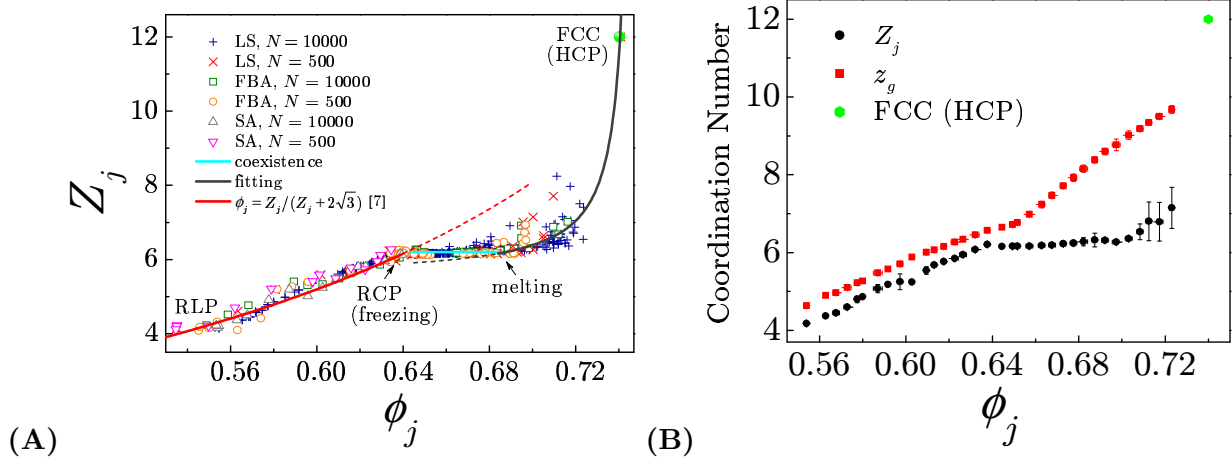


FIG. 5: **(A)** The mechanical coordination number Z_j versus the volume fraction ϕ_j with different system sizes (500 and 10,000 particles) and algorithms (Lubachevsky-Stillinger LS, force-biased FBA, and split SA algorithms). The results show that the transition does not depend on the system size and the algorithm used. **(B)** Comparison between geometrical coordination number z_g and mechanical coordination number Z_j . Along the disordered branch, z_g closely follows the mechanical coordination number Z_j . We expect that in the thermodynamical limit the gap between both coordinations may diminish. z_g and Z_j start to diverge at RCP, which is an indication of increasing geometric degeneracies in the contact network at the onset of crystallization.

within the system error. The pressure of the packings at the jamming point studied in this paper is 100 ± 8 KPa. The difference between the volume fraction ϕ of these packings and the critical volume fraction ϕ_j from power-law fitting in Eq. (4) is about 10^{-3} .

The same preparation protocol is repeated by using the force-biased algorithm (FBA) of [13] as initial protocol. The force-biased algorithm is a variant of the original method of W. S. Jodrey and E. M. Tory, *Phys. Rev. A* **32**, 2347 (1985), We also generate packings following the split algorithm of [7] starting with low initial volume fractions at $\phi_i = 0.3$ below RLP.

The mechanical coordination number, Z_j , versus the final jamming density, ϕ_j , is plotted in Fig. 5A for all the obtained jammed packings which total 720. The plot signals the existence of a transition at RCP. It is analogous to the equilibrium liquid-solid transition in hard-spheres, if we replace Z_j by the kinetic pressure of the fluid [6].

II. OTHER ASPECTS OF THE RCP TRANSITION

A. Finite size analysis

It is important to determine the finite size effects of our results. Figure 5A shows the results for smaller systems of 500 particles compared with 10,000 spheres system used in Fig. 1. We find that both plots are consistent with each other. While Fig. 1 shows the average of Z_j over the LS packings, Fig. 5A shows each point representing a single packing obtained with the indicated algorithms for different system sizes. We find that the transition is similar over the different protocols.

B. Isostatic and geometrical coordination numbers and symmetry breaking

While the isostatic coordination number has been well documented at RCP [4, 14, 18], the possibility of states with $Z_j = 6$ along the coexistence region with $\phi_{\text{rcp}} < \phi_j < \phi_{\text{melt}}$ requires more elaboration [6]. We recall, however that the limiting condition $Z_{\text{iso}} = 6$ is necessary, but not sufficient, for a rigid isostatic aggregate: a kinematic condition for rigidity must hold [18] where the functions that describe the connections between the centers of contacting particles are independent. The presence of crystal-like regions suggests that this condition may not be satisfied. Thus, the packings with $Z_j = 6$ in the coexistence region are not necessarily isostatic, except exactly at the freezing point.

It is interesting to understand the geometrical rearrangements occurring during the RCP transition in light of the fact that the packings enter the coexistence region from RCP by keeping $Z_j = 6$ constant. The particles modify the positions of the 6 contacts in average at RCP to create crystal-like regions without creating new contacts or destroying old ones. This implies that the arrangements of particles are such that particles in the second coordination shell come closer to the central particle and contribute to the first coordination shell, yet without producing a new contacting force since Z_j is kept at 6 in the entire coexistence region. The new particles moving into the first coordination shell can be considered in geometrical contact but carrying no force. Thus following [7] we introduce the idea of geometrical contact, z_g , as those particles in the first coordination shell that do not provide any force but still are close enough to the central particle to contribute to the geometrical contact network. The geometrical coordination number z_g is different from the mechanical

coordination number Z_j which only counts those contacts with nonzero forces. By definition $z_g \geq Z_j$.

While Z_j is easy to measure in computer simulations of soft particles as the number of contacts between overlapping particles, the geometrical coordination number, z_g , can be measured by slightly inflating the spheres up to 4% of their diameters and counting the resulting contact particles, as discussed in [7]. In practice, the geometrical coordination number measures the particles surrounding a central one with a gap between them from zero or negative (giving Z_j) up to $\delta = 0.08R$ as discussed in [7]. We notice that $\delta = 0.08R$ is much smaller than the location of the second peak in the radial distribution function which occurs around $\delta \sim 2R$. The value $\delta = 0.08R$ is specific for a system of $N=10,000$. We expect this value to diminish in the thermodynamic limit.

Figure 5B plots the geometrical and mechanical coordination z_g and Z_j as a function of ϕ_j for the same packings as in Fig. 1. We find that along the disordered branch, $z_g \approx Z_j$ as expected [7]. However, in the coexistence region, $Z_j = 6$ stays constant while z_g keeps growing with ϕ_j . The separation between z_g and Z_j is a signature of the onset of ordering at the freezing point. As explained above, the system starts to crystallize by allowing particles in the second coordination shell to come closer to the central particle and moving the Z_j contacting particles towards a FCC arrangement. At the melting point, the condition $Z_j = 6$ cannot hold any longer and the system transitions to the other branch with an increase of Z_j up to 12.

The distinction between z_g and Z_j is not only important for a characterization of the transition. It is also important to interpret the experimental results. Due to the uncertainty in detecting the exact position of the particles in any experiment, the exact mechanical coordination might be very difficult to obtain. Thus, a small uncertainty in the determination of the contacting particles $\delta = 0.08R$ will produce z_g as shown in Fig. 5B. One way to obtain the actual mechanical coordination from experimental data is to use the experimentally obtained coordinates of the particles as initial positions of a MD simulation using Hertz-Mindlin forces to relax the configurations and find the exact force balance network of the packing. Codes to develop this procedure are available at www.jamlab.org. We also provide most of the packings used in this study as well as the code to calculate the entropy.

C. Relation to the glass transition

The thermodynamic character of the RCP transition seemingly contrasts to the non-thermodynamic viewpoint of the glass transition which proposes a dynamical arrest upon supercooling [17]. However, the same phenomenology of vitrification could be applied to the RCP transition by extrapolating the entropy of the disordered branch $s(\phi_j)$ into a metastable region below the freezing point as schematically shown in Figs. 1 and 3B from $a \rightarrow b$. Two scenarios may emerge: the metastable branch may end in a metastability limit at the spinodal $\partial X/\partial S = 0$ [17] or it may continue until the entropy of the metastable liquid is zero as shown in Fig. 3B. Such a scenario would predict a Kauzmann density ϕ_K at which the entropy of the disordered branch vanishes, signaling the existence of an ideal jammed glass analogous to the Kauzmann temperature in glasses [6].

III. DESCRIPTIVE VIEWPOINT OF THE RCP TRANSITION

A. Orientational order parameter

The orientational order is measured by associating a set of spherical harmonics with every bond joining a sphere and its neighbors [19]:

$$Q_{lm}(\vec{r}) = Y_{lm}(\theta(\vec{r}), \phi(\vec{r})), \quad (6)$$

where the $\{Y_{lm}(\theta, \phi)\}$ are spherical harmonics, and $\theta(\vec{r})$ and $\phi(\vec{r})$ are the polar angles of the bond. The local orientational order parameter q_l for a particle i is given by rotationally invariant combinations of Q_{lm} ,

$$q_l = \left[\frac{4\pi}{2l+1} \sum_{m=-l}^l |\overline{Q}_{lm,i}|^2 \right]^{1/2}, \quad (7)$$

where $\overline{Q}_{lm,i}$ is averaged over N_i neighbors of this particle,

$$\overline{Q}_{lm,i} = \frac{1}{N_i} \sum_{j=1}^{N_i} Q_{lm}(\vec{r}_{ij}). \quad (8)$$

We also consider the global orientational order Q_l , as well as the third-order invariants W_l , which are

$$Q_l = \left[\frac{4\pi}{2l+1} \sum_{m=-l}^l |\overline{Q}_{lm}|^2 \right]^{1/2}, \quad (9)$$

where the average is taken over all the N_b bonds in the packing,

$$\overline{Q}_{lm} = \frac{1}{N_b} \sum_{bonds} Q_{lm}(\vec{r}), \quad (10)$$

and

$$W_l = \sum_{\substack{m_1, m_2, m_3 \\ m_1 + m_2 + m_3 = 0}} \begin{bmatrix} l & l & l \\ m_1 & m_2 & m_3 \end{bmatrix} \times \overline{Q}_{lm_1} \overline{Q}_{lm_2} \overline{Q}_{lm_3}, \quad (11)$$

where the coefficients $\begin{bmatrix} l & l & l \\ m_1 & m_2 & m_3 \end{bmatrix}$ are the Wigner 3j symbols.

We use a definition of bond as in [19] where all spheres within $r_c = 1.2d$ of a given sphere are near neighbors, where $d = 2R$ is the sphere diameter. We note that $r_c = 1.2d$ is the center of the first peak (centered at $r = 0$) and the second peak (centered at $r = 1.4d$) in the radial distribution function $g(r)$ of a perfect FCC lattice. Thus, this criteria is also consistent with the definition used in T. M. Truskett, S. Torquato, P. G. Debenedetti, *Phys. Rev. E* **62**, 993 (2000), where r_c is the first minimum in $g(r)$. The neighbors can also be defined as those who have mechanical contacts with the given sphere, Z_j . The basic results do not change by changing the definition of nearest neighbors. The results of the global orientational order Q_l and W_l are shown in Fig. 2A and Fig. 2B. To investigate the structures of the phases, Fig. 2C plots the probability distribution $P(q_6)$, which is the most sensitive measure of the local order parameters.

B. Orientational correlation function

The bond-angle correlation functions (Fig. 6) can be obtained via [19]:

$$G_l(r) = \frac{4\pi}{2l+1} \sum_{m=-l}^l \langle Q_{lm}(\vec{r}) Q_{lm}(\vec{0}) \rangle, \quad (12)$$

where the angular bracket indicates an average over all particles separated by \vec{r} . A non-zero asymptotic value of $G_6(r)$ implies a long-range correlation in the orientational order. From Fig. 6, it is clear that the crystal phase has long-range orientational order, while no order can be found in the random phase.

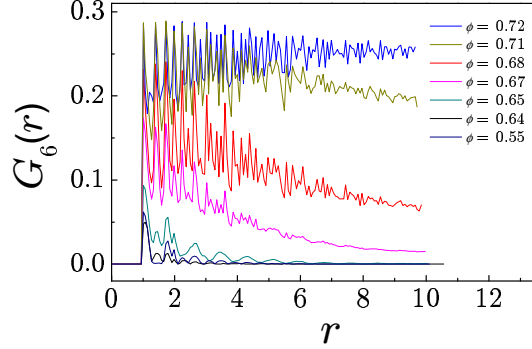


FIG. 6: The orientational correlation function Eq. (12) for different packings with ϕ_j . $G_6(r)$ vanishes at large r below $\phi_j = 0.64$, while it approaches a nonzero constant when $\phi_j > 0.64$. The nonzero asymptote of $G_6(r)$ is a signature of long-range correlation of orientational order. RCP is a well defined singularity at $\phi_j = 0.64$ where the orientational symmetry breaking occurs.

C. Local orientational disorder

We have established that crystalline structures appear in the coexistence region and solid-like branch. The remaining question is what kind of lattice structure dominates in the crystallized packings. Since the differences of the orientational order parameters, especially Q_6 , are not significant between different perfect lattice clusters (such as the icosahedral, FCC, HCP, BCC, and SC clusters, see [19], Fig. 2) we apply another measure, the local orientational disorder, to identify the crystalline nuclei as defined in M. Bargiel and E. M. Tory, *Adv. Powder Technol.* **12**, 533 (2001).

For a given sphere i , let θ_{ijk} be the angle between the j th and k th neighbors. Furthermore let θ_{jk}^{fcc} , θ_{jk}^{hcp} , $\theta_{jk}^{\text{icos}}$ be similarly calculated angles for the perfect 13-sphere fragments of FCC, HCP and icosahedral packings, θ_{jk}^{bcc} be the angles for the 8-sphere fragment of a perfect BCC packing, and θ_{jk}^{sc} be the angles for the 6-sphere fragment of a perfect SC packing. The local disorders are defined as following:

$$\theta_i^{\text{fcc}} = \sqrt{\frac{1}{66} \sum_{j=1}^{11} \sum_{k=j+1}^{12} (\theta_{ijk} - \theta_{jk}^{\text{fcc}})^2}, \quad (13)$$

$$\theta_i^{\text{hcp}} = \sqrt{\frac{1}{66} \sum_{j=1}^{11} \sum_{k=j+1}^{12} (\theta_{ijk} - \theta_{jk}^{\text{hcp}})^2}, \quad (14)$$

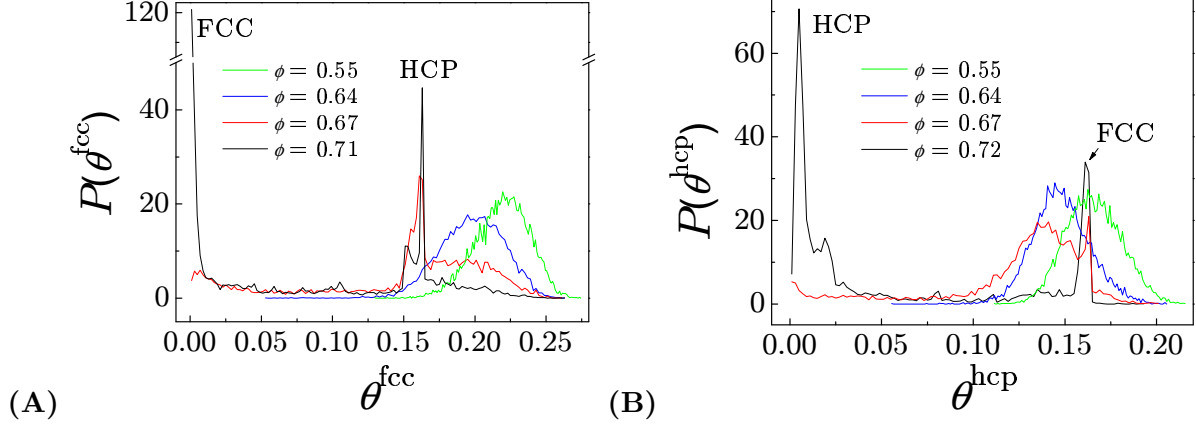


FIG. 7: **(A)** Distributions of local disorder θ_i^{fcc} defined in Eq. (13) for packings with different ϕ_j as indicated. The distribution functions below $\phi_j = 0.64$ are Gaussian, the center of the peak moves to $\theta_i^{\text{fcc}} = 0.2$ as the volume fraction ϕ_j approaches 0.64. This disordered peak decreases above $\phi_j = 0.64$ and seems to disappear above $\phi_j = 0.68$. Two ordered peaks appear after RCP, the one at $\theta_i^{\text{fcc}} = 0$ corresponds to FCC structure, while the other one at $\theta_i^{\text{fcc}} = 0.16$ corresponds to HCP. The peak at zero eventually evolves to a delta function as the packing structure approaches a perfect FCC. We use the median of the FCC peak and the disordered peak at $\phi_j = 0.64$ as a cutoff to identify local FCC structure, ie., particles with $\theta_i^{\text{fcc}} < \theta_c^{\text{fcc}}$ are defined as FCC crystalline nuclei, where $\theta_c^{\text{fcc}} = 0.1$. **(B)** Distributions of local disorder θ_i^{hcp} defined in Eq. (14) for packings with different ϕ_j as indicated. The distribution functions have similar behavior as those of θ_i^{fcc} . The cutoff $\theta_c^{\text{hcp}} = 0.075$ is used to identify HCP crystalline nuclei.

$$\theta_i^{\text{icos}} = \sqrt{\frac{1}{66} \sum_{j=1}^{11} \sum_{k=j+1}^{12} (\theta_{ijk} - \theta_{jk}^{\text{icos}})^2}, \quad (15)$$

$$\theta_i^{\text{bcc}} = \sqrt{\frac{1}{28} \sum_{j=1}^7 \sum_{k=j+1}^8 (\theta_{ijk} - \theta_{jk}^{\text{bcc}})^2}, \quad (16)$$

$$\theta_i^{\text{sc}} = \sqrt{\frac{1}{15} \sum_{j=1}^5 \sum_{k=j+1}^6 (\theta_{ijk} - \theta_{jk}^{\text{sc}})^2}. \quad (17)$$

Note that to calculate the values properly, we first need to sort the angles θ_{ijk} , θ_{jk}^{fcc} , θ_{jk}^{hcp} , $\theta_{jk}^{\text{icos}}$, θ_{jk}^{bcc} and θ_{jk}^{sc} , and then compare them one by one. Also note that the BCC and SC clusters have fewer neighbors than FCC, HCP and icosahedral clusters.

Since the θ_i 's measure the local disorder in the packings compared to a particular lattice structure, a perfect lattice cluster would have a zero value of θ . Any packing with significant amount of certain lattice clusters would indicate a peak centered around the origin in the distribution function of the local disorder θ_i corresponding to that particular lattice.

The distribution of FCC clusters $P(\theta_i^{\text{fcc}})$ for packings with different ϕ_j is shown in Fig. 7A. We find that FCC and HCP dominate in the crystalline packings for $\phi_j \geq \phi_{\text{melt}}$. Indeed we observe two prominent peaks in the distribution, one at FCC $\theta_i^{\text{fcc}} = 0$ and the other at HCP $\theta_i^{\text{fcc}} = 0.16$, while BCC, SC and icosahedral ordering are negligible. The FCC peak dominance indicates that the majority of the clusters are FCC with a small proportion of HCP clusters. Similar to the distributions of local orientational orders shown in Fig. 2C, we find no crystalline clusters in the random packings as evidenced by the Gaussian distributions of $P(\theta_i^{\text{fcc}})$ for $\phi_j \leq \phi_{\text{rcp}}$ as seen in Fig. 7A. In the coexistence region, the distributions are formed by a linear combination of different phases at melting and freezing. The distribution of HCP clusters $P(\theta_i^{\text{hcp}})$ has similar behavior as $P(\theta_i^{\text{fcc}})$, as showed in Fig. 7B.

D. Cluster analysis of crystalline regions and correlation length

We are able to define crystalline or nearly crystalline clusters in a packing based on the local orientational disorder and mechanical contacts, and visualize them in a 3d plot. The clusters are defined as follows: First, each node in the clusters is a sphere with $\theta_i^{\text{fcc}} < \theta_c^{\text{fcc}}$ or $\theta_i^{\text{hcp}} < \theta_c^{\text{hcp}}$, where $\theta_c^{\text{fcc}} = 0.1$ and $\theta_c^{\text{hcp}} = 0.075$, as determined in Fig. 7. The definition ensures that the first peak in $P(\theta_i^{\text{fcc}})$ at zero in the distribution function of Fig. 7A is included in this consideration (as well as the analogous analysis for HCP). Next, if any two nodes are in mechanical contact, we build a link between the two nodes. Then the crystalline clusters are those nodes that are linked together. The clusters are visualized in Fig. 1.

Based on the definition of the crystalline clusters, the size of the largest cluster in the system and the correlation length of the clusters, ξ , are measured near the melting point. To calculate the correlation length, we first introduce the radius of gyration, $R_g(s)$, of a cluster consisting of s particles:

$$R_g^2(s) = \frac{1}{2s^2} \sum_{i,j} (\vec{r}_i - \vec{r}_j)^2, \quad (18)$$

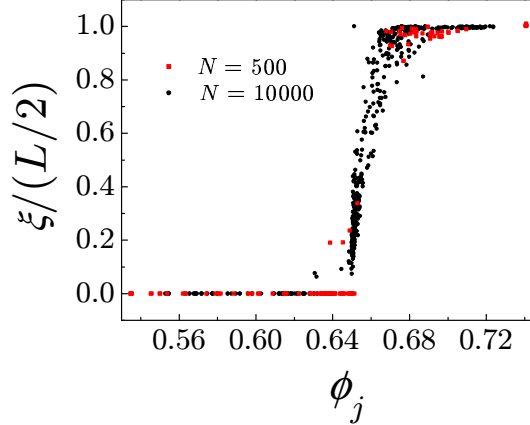


FIG. 8: Correlation length ξ of crystalline clusters. To calculate the correlation length, we first introduce the radius of gyration, $R_g(s)$, of a cluster consisting of s particles. The correlation length of a perfect FCC lattice with periodic boundary condition is $L/2$, where L is the system size, so the correlation length is scaled by $L/2$ in the figure. The crystalline clusters start to percolate at $\phi_j = 0.68$ as $\xi/(L/2)$ reaches a plateau with value 1. The results also show that the percolation at ϕ_{melt} does not depend on the system size.

then the correlation length is given by

$$\xi^2 = \frac{2 \sum_s R_g^2(s) s^2 n_s}{\sum_s s^2 n_s}, \quad (19)$$

where n_s is the number of clusters of size s in the packing.

The correlation length ξ of the crystalline clusters is measured near the melting point. Figure 8 confirms the linear increase of the size of crystals along the coexistence region from the freezing point where $\xi = 0$ to the melting point. When the system melts at ϕ_{melt} , ξ reaches a plateau consistent with the system size.

E. Radial distribution function

The radial distribution function $g(r)$ of the packing with volume fraction 0.72 in Fig. 9 shows all the peaks in FCC and HCP packings, which are indications of long range spatial order. On the other hand, the radial distribution functions of random packings only have two or three peaks (the second peak splits at $\phi_j = 0.64$), corresponding to short range order.

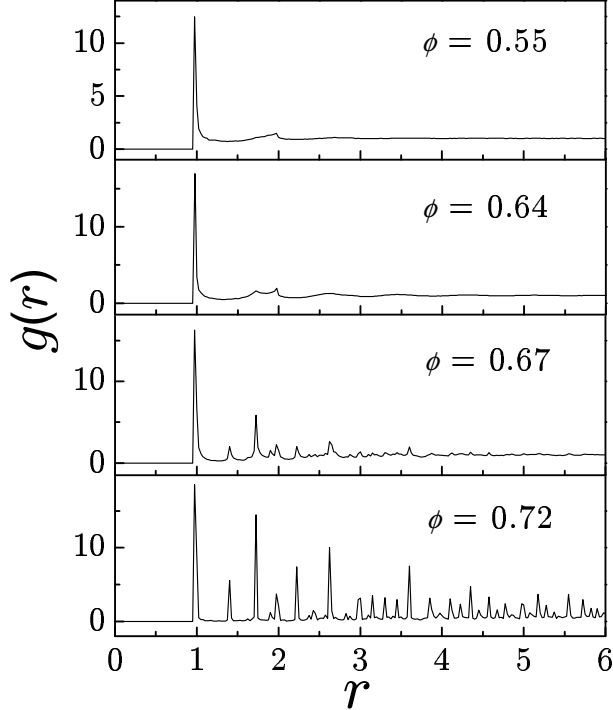


FIG. 9: Radial distribution functions $g(r)$ with different volume fractions ϕ_j . The figure clearly show the increasing of long range spatial order above $\phi_j = 0.64$.

In the coexistence region, $g(r)$ has more peaks than those of random packings, but the magnitude of the peaks decays very fast as the distance r becomes larger. The long-range order increases with the volume fraction in the coexistence region.

IV. THERMODYNAMIC VIEWPOINT OF THE RCP TRANSITION

A. Free energy

In the thermodynamics of jammed matter, the internal energy U is replaced by the volume W (usually called the volume function) [21]. Other thermodynamic potentials, such as enthalpy H , free energy F , Gibbs free energy G , are related to the volume function W as

$$H = W, \tag{20}$$

$$F = W - XS, \tag{21}$$

$$G = F = W - XS, \tag{22}$$

where X is the compactivity of the system and S the entropy, related as:

$$\frac{1}{X} = \frac{\partial S}{\partial W}. \quad (23)$$

Since thermodynamic pressure is not considered in our case, the volume W and enthalpy H are equivalent and the Helmholtz free energy F and Gibbs free energy G are identical, so that we refer to them only as the free energy. The differentials of the thermodynamic potentials are

$$dW = XdS + \mu dN, \quad (24)$$

$$dF = -SdX + \mu dN, \quad (25)$$

where μ is the chemical potential and N is the number of particles.

The free energy F , or Gibbs free energy G is equal to the product of N and μ ,

$$F = G = N\mu. \quad (26)$$

The free energy and chemical potential are continuous in the first order phase transition. On the other hand, the derivative of the chemical potential, $S = -\frac{\partial \mu}{\partial X}$, is discontinuous in a first order phase transition.

The compactivity X , as well as the entropy density $s = S/N$, can be calculated from the fluctuations of the Voronoi volumes, which is an analogy of the Edwards theory to the standard Boltzmann statistical mechanics. The definition of a Voronoi cell is a convex polygon whose interior consists of all points closer to a given particle than to any other. The Voronoi volume of a given particle, V_{vor} , is the volume of such a Voronoi cell (see [7] for more details).

We define the Voronoi fluctuations as $\sigma^2 \equiv \langle w_{\text{vor}}^2 \rangle - \langle w_{\text{vor}} \rangle^2$, where $w_{\text{vor}} = V_{\text{vor}}/V_g$ is the reduced Voronoi volume of each particle and the average is done over all the particles in a packing. The quantities $\sigma_1(\phi_j)$ and $\sigma_2(\phi_j)$ denote the Voronoi fluctuations in the disordered and ordered phases, respectively, as a function of ϕ_j .

We use the Einstein fluctuation theorem for jammed matter which is obtained from the similar relation in equilibrium systems by replacing the energy by the volume fluctuations [23–25]:

$$\langle(\delta W)^2\rangle = k_B X^2 \frac{\partial W}{\partial X}. \quad (27)$$

Here we assume that k_B plays the role of the Boltzmann constant in thermodynamics. Its value could be set to unity without changing the obtained results since in this context it just defines the units of entropy (in the main text we set $k_B = 1$ to simplify). This means that we measure the compactivity in units of volume V_g and that the entropy, which has units of k_B , is dimensionless. In terms of the Voronoi fluctuation σ and volume fraction ϕ_j , Eq. (27) reads:

$$\sigma_i^2 = -\frac{k_B}{V_g} \left(\frac{X}{\phi_j}\right)^2 \frac{\partial \phi_j}{\partial X}, \quad i = 1, 2. \quad (28)$$

Equation (28) applies to the disordered and ordered branches, σ_1 and σ_2 , separately. It does not apply to the coexistence region, since it requires the pure phases to calculate the fluctuations.

Using Eq. (28) we can calculate the thermodynamic quantities by integration. We first obtain the compactivity from:

$$\frac{1}{X(\phi_j)} = \frac{k_B}{V_g} \int_{\phi_{\text{rlp}}}^{\phi_j} \frac{d\phi}{\phi^2 \sigma_1^2(\phi)} + \frac{1}{X_{\text{rlp}}}, \quad \phi_{\text{rlp}} \leq \phi_j \leq \phi_{\text{rcp}}, \quad (29a)$$

$$\frac{1}{X(\phi_j)} = \frac{k_B}{V_g} \int_{\phi_{\text{melt}}}^{\phi_j} \frac{d\phi}{\phi^2 \sigma_2^2(\phi)} + \frac{1}{X_{\text{melt}}}, \quad \phi_{\text{melt}} \leq \phi_j \leq \phi_{\text{fcc}}, \quad (29b)$$

where $X_{\text{melt}} = X(\phi_{\text{melt}})$ is the compactivity of the packing at the melting point and $X_{\text{rlp}} = X(\phi_{\text{rlp}})$ at RLP.

The entropy density is then obtained by a second integration using the definition Eq. (23) which reads:

$$\frac{1}{X} = -\frac{\phi_j^2}{V_g} \frac{\partial s}{\partial \phi_j}. \quad (30)$$

We integrate Eq. (30) for each branch to obtain:

$$s(\phi_j) = s_{\text{rcp}} + V_g \int_{\phi_j}^{\phi_{\text{rcp}}} \frac{d\phi}{X(\phi)\phi^2}, \quad \phi_{\text{rlp}} \leq \phi_j \leq \phi_{\text{rcp}}, \quad (31a)$$

$$s(\phi_j) = V_g \int_{\phi_j}^{\phi_{\text{fcc}}} \frac{d\phi}{X(\phi)\phi^2}, \quad \phi_{\text{melt}} \leq \phi_j \leq \phi_{\text{fcc}}. \quad (31b)$$

The entropy of FCC, s_{fcc} , is zero in the thermodynamic limit.

Equations (29) and (31) require three constants of integration: X_{rlp} , X_{melt} and the entropy of RCP: s_{rcp} . We now introduce three extra constraints to close the system. First, there are two conditions for equilibrium between two phases in jammed matter [17, 21]: (a) “thermal” equilibrium

$$X_{\text{melt}} = X_{\text{rcp}} \equiv X_c, \quad (32)$$

where X_c is the critical compactivity at the transition. (b) The equality of the chemical potentials of the two phases at the melting and the freezing RCP point: $\mu_{\text{melt}} = \mu_{\text{freez}}$ due to the conservation of number of particles. This is analogous to the equality of the free energy density at the transition from Eq. (26), which allows to calculate the entropy at the freezing point via $f_{\text{melt}} = f_{\text{rcp}}$:

$$s_{\text{rcp}} = s_{\text{melt}} + V_g \left(\frac{\omega_{\text{rcp}} - \omega_{\text{melt}}}{X_c} \right), \quad (33)$$

and the entropy of fusion is then:

$$\Delta s_{\text{fus}} \equiv s_{\text{rcp}} - s_{\text{melt}} = V_g \left(\frac{\omega_{\text{rcp}} - \omega_{\text{melt}}}{X_c} \right). \quad (34)$$

The final constant of integration to be obtained is the compactivity at the RLP point. As a first order approximation, X_{rlp} can be taken as infinite as has been shown in previous experimental and numerical studies [23, 25]. However, when we compare the obtained entropy Eq. (31) with an independent measure of the entropy using Shannon information theory (explained below) we find that there are slightly differences between both values of the entropy. Therefore, we consider X_{rlp} as a fitting parameter to be obtained by fitting the result of Eq. (31) with the Shannon entropy which in principle does not require any integration constant to be calculated. We note that using the fitted value of X_{rlp} instead of infinity does not change the final results, specifically the values of X_c and the entropy of fusion, even though the obtained X_{rlp} is “far” from infinite.

We summarize the calculation as follows: (a) We assume a value of X_{rlp} (which is later fitted with Shannon entropy) and integrate Eq. (29a) from RLP to ϕ_{rcp} and obtain the compactivity $X_{\text{rcp}} = X(\phi_{\text{rcp}})$. (b) Using Eq. (32) we obtain X_{melt} (or X_c). (c) Using X_{melt} , we integrate Eq. (29b) to obtain the $X(\phi_j)$ in the ordered branch, thus completing the calculation of the compactivity equation of state. (d) We integrate Eq. (31b) up to ϕ_{melt} to obtain the entropy of the melting point: s_{melt} . (e) Using Eq. (33) we obtain the entropy at

RCP, s_{rcp} . (f) This value is then plugged into Eq. (31a) to finish the calculation of $s(\phi_j)$ by a final integration. The above procedure is repeated for different values of X_{rlp} starting from infinite up to a finite value that will match the Shannon entropy as discussed below.

B. Shannon entropy

Entropy of jammed matter can be calculated in two different ways: (i) The entropy from fluctuation theory explained above. (ii) The entropy from information theory [23], so called "Shannon entropy", related to configurational disorder since topologically equivalent structures are considered as the same state. Shannon entropy attempts to measure the disorder in a string of information as defined in the seminal work of Shannon. This concept has been adapted to the measurement of the configurational entropy in physical systems defined through a contact network by Vink and Barkema [R. L. C. Vink, G. T. Barkema, *Phys. Rev. Lett.* **89**, 076405 (2002)]. In this work it was shown that the entropy obtained from the thermodynamic integration of fluctuations (or equivalently the specific heat) and the Shannon entropy are equivalent and accurately describe amorphous silicon and vitreous silica networks. The method has been extended to calculate the entropy of packings of granular materials in [23]. Below we explain the main details.

The advantage of the Shannon entropy calculation over the thermodynamic integration is that it does not require a constant of integration as in Eq. (31). For each state of jammed matter, we associate a probability of occurrence p_i to the state, which is calculated as follows.

We use the Voronoi cell and Delaunay triangulation for each particle to define a Voronoi network by considering contacts when a Voronoi side is shared between two particles, and hence are Delaunay contacts. A graph is constructed as a cluster of n particles that are Delaunay contacts, and by means of graph automorphism [B. D. McKay, Nauty user's guide (version 1.5), Tech. Rep. TR-CS-90-02, Australian National University (1990)] can be transformed into a standard form or "class" i of topologically equivalent graphs with a probability of occurrence $p(i)$. In practice, we determine $p(i)$ by extracting a large number m of clusters of size n from the system and count the number of times, f_i , a cluster i is observed, such that:

$$p(i) = f_i/m. \tag{35}$$

Then the Shannon entropy is defined as:

$$H(n) = - \sum p_i \ln p_i, \quad (36)$$

where we have again assumed the ‘‘Boltzmann-like’’ constant in front to be one. The Shannon entropy density is obtained as:

$$s_{\text{shan}} = \lim_{n \rightarrow \infty} [H(n+1) - H(n)], \quad (37)$$

by linear fitting of the extensive part of the Shannon entropy.

In general, the fluctuation entropy from Eq. (31) is greater than the Shannon entropy from Eq. (37) because Shannon entropy only counts configurational disorder and additional entropy could arise from freedom to move grains within the clusters of n particles without disrupting the Delaunay network. However, we discover that the fluctuation entropy obtained from Eq. (31) and Shannon entropy from Eq. (37) only differ by a scaling constant $k = 0.1$, ie., $ks = s_{\text{shan}}$, see Fig. 3B. Beyond this multiplicative constant the agreement between both estimations of the entropy is very good. Due to finite size effects the Shannon entropy also gives a nonzero value of the entropy of FCC, $s_{\text{fcc}} = 0.6$. This value is subtracted from the calculations. By fitting s_{shan} with the thermodynamic entropy we obtain the final constant of integration in Eq. (29a), $X_{\text{rlp}} = 0.5V_g$. While it is obvious that this constant is far from the infinite value which is expected and used in [23, 25] for the RLP limit, we notice that our final results are not very sensitive to the exact value of X_{rlp} . For instance, by setting $X_{\text{rlp}} \rightarrow \infty$ the fitting of the fluctuation entropy is slightly off in comparison with s_{shan} only in the vicinity of RLP but the values of X_c and the entropy of fusion do not have appreciable change.

Figure 4 in the main text shows the thermodynamic quantities in the first order phase transition of jammed matter. They are consistent with the general thermodynamic picture. Figure 10 plots the entropy versus w showing a linear dependence in the coexistence region. The entropy is an interpolation of the form: $s_x = xs_{\text{melt}} + (1-x)s_{\text{freez}}$ where x is the concentration of crystal clusters in the coexistence. Since $X = \partial W / \partial S$, the linearity of s between 0.64 and 0.68 is a manifestation of the coexistence of two phases at a constant X_c .

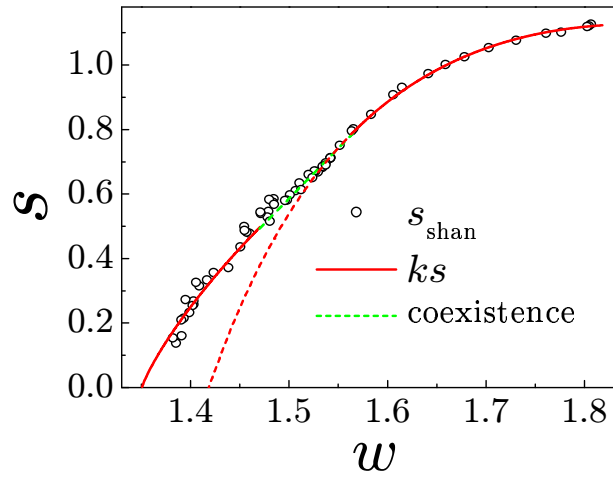


FIG. 10: Entropy versus reduced volume function $\omega = 1/\phi_j$.